Huang *et al. Complex Eng Syst* 2023;3:2
DOI: 10.20517/ces.2022.43

Complex Engineering Systems

Research Article

Open Access

Generation of high definition map for accurate and robust localization

Zhengjie Huang[1], Sijie Chen[1], Xing Xi[1], Yanzhou Li[1], Ya Li[2], Shuanglin Wu[3]

[1]School of Automation, Guangdong University of Technology, Guangzhou 510006, Guangdong, China.
[2]Ningbo Artificial Intelligence Institute, Shanghai Jiaotong University, Ningbo 315000, Zhejiang, China.
[3]State Key Laboratory of Acoustics, Institute of Acoustics, Chinese Academy of Sciences, Beijing 100190, China.

Correspondence to: Dr. Yanzhou Li, School of Automation, Guangdong University of Technology, No.100, Waihuan Xi Road, Guangzhou 510006, Guangdong, China. E-mail: lyz19921207@163.com

How to cite this article: Huang Z, Chen S, Xi X, Li Y, Li Y, Wu S. Generation of high definition map for accurate and robust localization. *Complex Eng Syst* 2023;3:2. http://dx.doi.org/10.20517/ces.2022.43

Received: 17 Oct 2022 **First Decision:** 24 Nov 2022 **Revised:** 2 Dec 2022 **Accepted:** 11 Jan 2023 **Published:** 31 Jan 2023

Academic Editor: Hamid Reza Karimi **Copy Editor:** Fanglin Lan **Production Editor:** Fanglin Lan

Abstract

This paper presents a framework for generating high-definition (HD) map, and then achieves accurate and robust localization by virtue of the map. An iterative approximation based method is developed to generate a HD map in Lanelet2 format. A feature association method based on structural consistency and feature similarity is proposed to match the elements of the HD map and the actual detected elements. The feature association results from the HD map are used to correct lateral drift in the light detection and ranging odometry. Finally, some experimental results are presented to verify the reliability and accuracy of autonomous driving localization.

Keywords: High definition map, factor graph optimization, localization, reprojection error

1. INTRODUCTION

In recent years, vehicle localization has been treated as an important part of an autonomous driving system. However, conventional odometry methods have drift problems with long-term use. An inertial navigation system (INS) will likely fail in scenarios with poor GNSS signals, such as tunnel and urban canyon scenarios [1]. For the sake of more accurate localization, multisensor fusion is developed to compensate for the respective deficiencies of various sensors. HD maps, as stable prior information, can provide reliable location constraints.

Fusion localization methods based on HD maps have been a significant research hotspot in recent years.

For HD maps, some computer-aided generation methods have emerged[2,3]. However, lane lines obtained using these methods are a series of 2-dimensional point sets, which occupy large storage space and do not carry elevation information. Some researchers store road features in point clouds and use point cloud registration methods to determine vehicle positions[4,5]. However, point cloud formats have disadvantages such as high coupling, difficulty in maintaining, and unfavorable object classification. For localization, some researchers reduce localization errors by matching road surface features, e.g. manhole covers[6–12]. However, the visibility of road features is easily affected by illumination, which makes the matching performance differ greatly at different times and results in unstable localization.

In this paper, the main work focuses on two aspects: First, a computer-aided generation method for HD maps is proposed. Currently, most papers consider the lane lines are in 2D plane when the lane line fitting is implemented. These methods are almost unusable in scenarios such as overpasses and culverts[13–16]. To broaden the use of HD maps, it is necessary to develop 3D fitting lane lines. Second, an accurate multisensor fusion localization method using generated HD map and existing odometry is proposed. It is worth noting that cumulative errors will occur if the localization method is only based on odometry. Thus, a positional constraint that has no connection with error is required to correct the estimated position. The contributions of this paper are summarized as follows:

1. We propose a method based on an iterative approximation to generate the 3D curve of lane lines. The spatial parameterized curve fitted by the proposed algorithm, which is global C^1 continuous, has broader applicability than the 2D curve equation. This method not only effectively reduces the number of parameters of the spline curve but also ensures the accuracy of the curve.
2. We separate the lanes and store them in a particular HD map format instead of holding them as semantic information in a point cloud. For the HD maps nonuniform sampling point problem, a method based on numerical integration is proposed to achieve uniform sampling over the arc length.
3. We propose a method to associate the elements in the HD map and the other elements in the perception results.In this paper, the basic elements of the HD map and the complete feature associations are formulated with their respective similarity evaluation metrics, considering the matching time, similarity and local structure consistency.
4. We transform the localization problem of fusing HD maps into a graph optimization problem. Based on the HD map and perceptual image feature association results, a lateral constraint is applied to the odometry localization results, and accurate, low-cost localization results are obtained.

2. RELATED WORKS

2.1. Generation of lane curve equations

Chen *et al.*[14] demonstrated that a cubic Hermite spline (CHS) can describe line segments, arc curves, and clothoids simultaneously and is a good choice for fitting lane lines. A CHS has at least C^1 continuity, which is more accurate in describing lane curves than a traditional segmented linear fold representation. Its uniform form allows fitting any lane curves parametrically using a sequence of feature points. Jo *et al.*[15] proposed a B-spline fitting method based on the optimal smoothing technique. Zhang *et al.*[16] proposed a lane line fitting method that considered a vehicle model to generate globally C^1 continuous lane lines that match the driving trajectory. Gwon *et al.*[17] proposed a segmented polynomial fitting method with sequential approximation, which outperformed B-spline and clothoid curves in terms of computational efficiency and modifiability.

2.2. Existing HD map formats

There is no unified standard for HD map formats, and various institutions and companies use different formats. The OpenDRIVE standard, developed by the Association for Standards in Automation and Measurement Sys-

tems (ASAM), has been used in simulations for some time and has good landing performance in some assisted driving models. The Navigation Data Standard (NDS) is a standard format for vehicle-level navigation databases jointly developed and published by vehicle manufacturers and automotive suppliers. The NDS format enables sharing of navigation data between different systems by separating the navigation data from the navigation software. Although OpenDRIVE and NDS are formats developed by more authoritative organizations, they need to be more open, as they provide only partial information to most developers. Therefore it is challenging to use them in practice[18,19].

Apollo OpenDRIVE is a modified version of OpenDRIVE to accompany the Baidu Apollo autonomous driving system. Instead of using geometric elements, it uses sequences of points to represent road elements. In addition, Apollo OpenDRIVE stores reference lines on the map and then describes the lane lines relative to the reference lines. This allows Apollo OpenDRIVE to express maps with higher accuracy than OpenDRIVE for the same map file size and also facilitates some calculations in the subsequent planning module.

In 2018, Poggenhans *et al.*[20] released the open source Lanelet2. Based on the OpenStreetMap (OSM) format, Lanelet2 has been extended and allowed direct access to many of the open source tools that accompany OSM. Benefiting from its complete toolkit, open architecture, and easily editable features, Lanelet2 not only allows the storage of information about roads, road signs, light poles, and buildings with precise geometry but also enables lane level and traffic-compliant routing.

2.3. Multisensor fusion localization

GNSS are widely spread in intelligent transport systems and offer a low-cost, continuous and global solution for positioning[21]. It can provide a more stable location. GNSS localization system has obvious disadvantages: significant errors and easy to be obscured. Therefore, scholars have increasingly recognized multisensor fusion as necessary in recent years. Simultaneous localization and mapping (SLAM) is a technology that constantly builds and updates environmental information by sensing things in an unknown environment while tracking their position in the background. SLAM is generally divided into light detection and ranging (LiDAR)-based SLAM, such as LOAM[22], LeGO-LOAM[23], LINS[24], and LIO-SAM[25], and vision-based SLAM, such as ORB-SLAM[26], VINS[27,28]. If the localization relies solely on LiDAR or cameras, position estimation errors will accumulate over a long time and distance. An HD map, as a globally consistent data source, can also provide reliable global location constraints. Multisensor fusion localization algorithms combined with HD map lane-level localization algorithms will be more accurate and have great potential.

2.4. Localization based on HD map

Scholars continue to reduce the error by matching pavement marking features or lane line curvature based on existing localization[6–12]. However, the visibility of road markings is affected by light. The visibility of different markings on the same road segment varies greatly at different periods, making it difficult to achieve stable positioning performance. At the same time, these efforts do not consider the common function of road elements in localization and planning, and these methods can only use the generated road elements in localization.

3. SYSTEM OVERVIEW

The proposed system consists of three parts. The first part is lane line fitting. An inverse lane line perspective mapping method combined with ground equations is discussed. An iterative approximation-based process of fitting piecewise CHS curves is proposed. This method satisfies the requirement of small data storage and ensures the continuity of lanes.

The second part is the HD map postprocessing. The data structure and coordinate system required for the HD

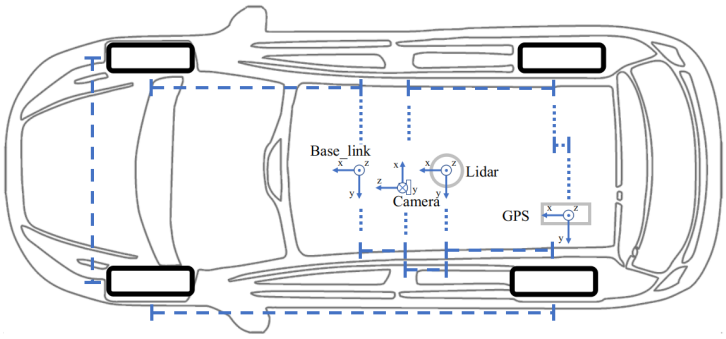

Figure 1. The coordinate system of the vehicle.

Figure 2. Lane detection data.

map are discussed. We use a numerical integration method to calculate the parametric curve arc lengths. In this way, the parametric scale equidistant curves are transformed into arc-length scale middle curves, making the curve structure more uniform.

The third part is a fusion localization method based on HD maps and odometry. A method for feature association between current HD map information and the camera's real-time perceptual features is investigated. A respective similarity evaluation metric is formulated for different essential elements in the HD map. According to the accumulated confidence smoothing, the results are smoothed on the time scale and converted into a graph optimization problem. Finally, the amount of computation for graphics optimization is reduced using a sliding window method and improved keyframe selection.

The KITTI dataset is used for autonomous driving and mobile robot research [29]. This study uses only camera 2 and the synchronized and corrected data in the KITTI dataset. Therefore, we add some definitions based on KITTI's original definitions. Taking camera 2 as the origin to establish a camera coordinate system, the intersection of the vertical line from the midpoint of the front and rear axles of the vehicle (the middle of the four wheels) to the ground and the ground is taken as the vehicle center point, and the base_link coordinate system is established. The positive direction of the x-axis is forward along the vehicle's driving path, the y-axis points to the left side of the vehicle's driving direction, and the z-axis is vertical upward. The vehicle's coordinate system is shown in Figure 1.

4. HD MAP GENERATION

We discuss the generation of HD maps with the lane line detection results already available from existing experimental data, and the test images are from the KITTI dataset [29]. An example of lane line data is shown in Figure 2. The lane line data are stored as line segments. Each segment is a lane consisting of several points.

4.1. Inverse perspective mapping with ground equation

The projection equation of the camera is as follows:

$$Z_{\mathrm{c}}\begin{bmatrix}\boldsymbol{P}_{\mathrm{uv}}\\1\end{bmatrix}=\boldsymbol{K}\boldsymbol{P}_{\mathrm{c}}=\boldsymbol{K}\boldsymbol{T}_{\mathrm{cb}}\boldsymbol{P}_{\mathrm{b}} \tag{1}$$

where $\boldsymbol{P}_{\mathrm{c}}=[X_{\mathrm{c}},Y_{\mathrm{c}},Z_{\mathrm{c}}]^{\mathrm{T}}$ is the coordinates of a point under the camera coordinate system, and $\boldsymbol{K}$ is the intrinsic matrix of the camera. $\boldsymbol{Z}_{\mathrm{c}}$ is the z-axis coordinate of the actual ground point in the camera coordinate system. $\boldsymbol{P}_{\mathrm{b}}$ is the coordinates of a point in the vehicle coordinate system, $\boldsymbol{P}_{\mathrm{uv}}=[u,v]^{\mathrm{T}}$ is the coordinates of a point in the pixel coordinate system, $\boldsymbol{T}_{\mathrm{cb}}$ represents transformation matrix from the camera to the vehicle coordinate system.

We calculate the ground equations in the LiDAR coordinate system as follows[30]:

$$\boldsymbol{n}_{\mathrm{l}}^{\mathrm{T}}\boldsymbol{P}_{\mathrm{l}}=\boldsymbol{n}_{\mathrm{l}}^{\mathrm{T}}\boldsymbol{T}_{\mathrm{lc}}\boldsymbol{P}_{\mathrm{c}}=\boldsymbol{n}_{\mathrm{c}}^{\mathrm{T}}\boldsymbol{P}_{\mathrm{c}}=-D \tag{2}$$

where $\boldsymbol{n}_{\mathrm{l}}$ is the vector normal to the ground plane in the LiDAR coordinate system, and $\boldsymbol{T}_{\mathrm{lc}}$ is the transformation matrix from the LiDAR to the camera coordinate system. $\boldsymbol{P}_{\mathrm{l}}$ is the point in the radar coordinate system. $\boldsymbol{n}_{\mathrm{c}}$ is the vector normal to the ground plane in the camera coordinate system.

Combining (1) and (2),

$$Z_c\begin{bmatrix}\boldsymbol{P}_{\mathrm{uv}}\\1\\0\end{bmatrix}=\begin{bmatrix}f_x&0&c_x&0\\0&f_y&c_y&0\\0&0&1&0\\A&B&C&D\end{bmatrix}\boldsymbol{P}_{\mathrm{c}}=\boldsymbol{M}\boldsymbol{T}_{\mathrm{cb}}\boldsymbol{P}_{\mathrm{b}} \tag{3}$$

where $\boldsymbol{M}$ is:

$$\boldsymbol{M}=\begin{bmatrix}\boldsymbol{K}&\boldsymbol{0}\\\boldsymbol{n}_{\mathrm{c}}^{\mathrm{T}}&D\end{bmatrix} \tag{4}$$

The physical meaning of D is the offset of the plane in the direction of the normal vector (after normalizing the normal vector $\boldsymbol{n}$). In the camera coordinate system, D in the ground equation cannot be zero. Therefore, it can be assumed that $\boldsymbol{M}$ is full rank.

Since the matrix $\boldsymbol{M}$ varies with the ground equation, its inverse matrix must be calculated for each subsequent frame, and the program overhead is significant. From the chunk matrix property, we can further obtain the following:

$$\frac{1}{Z_c}\boldsymbol{P}_{\mathrm{c}}=\begin{bmatrix}\boldsymbol{K}^{-1}&\boldsymbol{0}\\-D^{-1}\boldsymbol{n}_{\mathrm{c}}^{\mathrm{T}}\boldsymbol{K}^{-1}&D^{-1}\end{bmatrix}\begin{bmatrix}\boldsymbol{P}_{\mathrm{uv}}\\1\\0\end{bmatrix} \tag{5}$$

From (5), the program only needs to compute $\boldsymbol{K}^{-1}$ once in the initialization phase. Then, it is just a matter of computing $\boldsymbol{n}'^{\mathrm{T}}$ and D^{-1} in each subsequent frame of the program.

4.2. Piecewise cubic hermite spline fitting

A CHS curve is a cubic polynomial curve determined by the starting point p_0, the ending point p_1, the slope of the starting point d_0, and the slope of the ending point d_1. The equation of a parametric cubic polynomial curve is defined as:

$$\mathrm{F}_i(\boldsymbol{p}_i,\boldsymbol{p}_{i+1},\boldsymbol{d}_i,\boldsymbol{d}_{i+1},t)=\boldsymbol{P}_i\boldsymbol{H}\boldsymbol{t}=\begin{bmatrix}\boldsymbol{p_i}\\\boldsymbol{p_{i+1}}\\\boldsymbol{d_i}\\\boldsymbol{d_{i+1}}\end{bmatrix}^{\mathrm{T}}\begin{bmatrix}1-3t^2+2t^3\\3t^2-2t^3\\t-2t^2+t^3\\-t^2+t^3\end{bmatrix} \tag{6}$$

(6) represents the equation of the i-th segment of a CHS curve. A CHS curve has global C^1 continuity[16].

The problem of fitting the i-th segment of the curve to N_i points can be transformed into a minimization problem:

$$\min \sum_{k=0}^{N_i} \mathrm{err} = \min \sum_{k=0}^{N_i} \left\| \mathrm{F}_i(\boldsymbol{p}_i, \boldsymbol{p}_{i+1}, \boldsymbol{d}_i, \boldsymbol{d}_{i+1}, \boldsymbol{t}_i) - \boldsymbol{p}_{\boldsymbol{k}} \right\| \tag{7}$$

It is evident that in each segment of the curve except the first one, only the endpoint tangent vector $\boldsymbol{d}_{i+1}$ needs to be fitted. In (7), fitting a parametric curve equation needs to consider multiple minimization problems at the same time.

An algorithm for fitting a piecewise spatial CHS curve is proposed based on the idea of asymptotic approximation, as shown in the Algorithm 1. The main idea of the algorithm is to cyclically optimize $\boldsymbol{d_i}$, $\boldsymbol{d_{i+1}}$ and $\boldsymbol{t}$. That is, one parameter is optimized while keeping the other two parameters unchanged until each parameter is optimized N_{iter} times. To achieve global C^1 continuity, the vector tangent to the starting point of subsequent curves adopts the endpoint tangent vector of the previous segment. In this paper, $\mathrm{F}_i(\boldsymbol{d}_i)$ means that other quantities are left unchanged, and only $\boldsymbol{d}_i$ is changed, and the same is true for other variables. In this paper, the optimizer uses L-BFGS-B[31].

$$\begin{cases} \underset{\boldsymbol{d}_0, \boldsymbol{d}_1}{\arg\min} \sum_{k=0}^{N_0} \left\| \mathrm{F}_0(\boldsymbol{d}_0, \boldsymbol{d}_1) - p_k \right\| & i = 1 \\ \underset{\boldsymbol{d}_{i+1}}{\arg\min} \sum_{k=0}^{N_i} \left\| \mathrm{F}_i(\boldsymbol{d_{i+1}}) - p_k \right\| & i = 2, 3, \ldots N \end{cases} \tag{8}$$

Algorithm 1 CHS Curve Fitting with Asymptotic Approximation

N: Total number of curve segments.
i: The i-th curve, $i \in [1, N]$.
N_i: Point set size.
k: The k-th point in the set of points, $k \in [1, N_i]$.
t_k: The parameter corresponding to the kth point.
$\boldsymbol{t}_i$: The column vector consisting of t_k.
N_{iter}: Number of iterations.
for $i \in [1, N]$ **do**
  Initialization :$\boldsymbol{p}_i, \boldsymbol{p}_{i+1}$
  for $j \in [1, N_{\mathrm{iter}}]$ **do**
    $\boldsymbol{t}_i = \text{L-BFGS-B}\left(\underset{\boldsymbol{t}}{\arg\min} \sum_{k=1}^{N_i} \mathrm{F}_i(\boldsymbol{t}_k) \right)$
    if $i == 1$ **then**
      $\boldsymbol{d}_i = \text{L-BFGS-B}\left(\underset{\boldsymbol{d}_i}{\arg\min} \sum_{k=1}^{N_i} \mathrm{F}_i(\boldsymbol{d}_i) \right)$
    end if
    $\boldsymbol{d}_{i+1} = \text{L-BFGS-B}\left(\underset{\boldsymbol{d}_{i+1}}{\arg\min} \sum_{k=1}^{N_i} \mathrm{F}_i(\boldsymbol{d}_{i+1}) \right)$
  end for
end for
return F

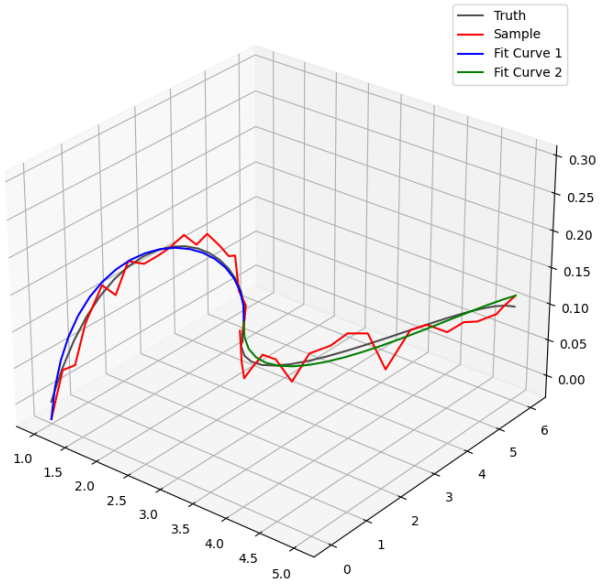

Figure 3. Curve fitting.

The traditional piecewise cubic Hermite interpolating polynomial (PCHIP)[32] algorithm fits a set of curves with four parameters every two points, so the number of parameters to be fitted increases exponentially with an increasing number of sampling points. The asymptotic approximation of the CHS curve fitting algorithm proposed in this section adds several sampling points to the curve fitting equation as constraint terms, which can effectively reduce the total number of parameters while ensuring that the curve is as close as possible to the remaining sampling points. As shown in Figure 3, the gray line is the actual curve, the red line is composed of 20 sampling points, and the blue and green lines are the curves fitted by the algorithm in this study. The smooth and continuous connection between the blue and green lines is evident in Figure 3. This shows that the algorithm's results in this study can still guarantee a certain accuracy in the case of more serious disturbances. This accuracy satisfies the need for lane line fitting.

4.3. Intersection completions

Considering that some roads prohibit left or right turns, it is not feasible to fix intersections through geometric relationships. In this study, we evaluate the intersection connection using the trajectory information of the vehicle driving. The vehicle driving trajectory is superimposed on the set of lane points. When the lane points near the vehicle driving route are less than a threshold value, the intersection is considered to be at that point.

The parameters of a CHS curve equation in an intersection (called virtual lanes) can be determined by combining the endpoint of the departure lane and its tangent vector with the start point of the entry lane and its tangent vector. That is, for the equation of virtual lanes at this intersection, the equation of a lane line in intersection F_I satisfies $F_I = F(\boldsymbol{p}_{prev}, \boldsymbol{p}_{next}, \boldsymbol{d}_{prev}, \boldsymbol{d}_{next}, t)$, where $\boldsymbol{p}_{prev}$ and $\boldsymbol{p}_{next}$ are the endpoint coordinates of the starting lane and the start point coordinates of the target lane, respectively, and $\boldsymbol{d}_{prev}$ and $boldsymbold_{next}$ are the endpoint tangent vector of the starting lane and the start point tangent vector of the target lane.

4.4. Arc length equalization of curves

In Lanelet2, a sequence of points is used to describe lane lines. This storage method has some advantages; path-planning algorithms with some processing can use this point sequence. In addition to manual adjustment to edit HD maps, they must also manipulate the point sequence and cannot be operated on the parameterized curve. In contrast, some scenarios require global smoothing of curves, such as lane visualization drawing.

Therefore, lane parameters and point sequences are stored in the map file in this study. Optimizing the curve equation after parameter t does not have a physical meaning. To make the spacing of sampling points on each section of the lane consistent, the arc length of the curve needs to be calculated and used to re-extract the equidistant sampling points.

The CHS arc lengths can be calculated from the following equation:

$$s = \int_0^1 g(t)\,\mathrm{dt} = \int_0^1 \sqrt{x'(t)^2 + y'(t)^2 + z'(t)^2}\,\mathrm{dt} = \int_0^1 \sqrt{\boldsymbol{t'}^{\mathrm{T}}\boldsymbol{H}^{\mathrm{T}}\boldsymbol{P}^{\mathrm{T}}\boldsymbol{P}\boldsymbol{H}\boldsymbol{t'}}\,\mathrm{dt} \tag{9}$$

(9) is an elliptic integral, which is difficult to calculate by ordinary methods. In this study, the Gauss-Kronrod quadrature method [33] is used to simplify the integration calculation process.

We use the G7-K15 method, a 7-point Gauss rule with a 15-point Kronrod rule, apply it to (9), and use the rules of the upper and lower limits of the integral transformation to calculate the arc length from t_0 to t_1:

$$\int_{t_0}^{t_1} g(x)\,\mathrm{dx} = \int_{-1}^{1} \frac{t_1 - t_0}{2} g\left(\frac{x+1}{2}(t_1 - t_0) + t_0\right)\mathrm{dx} \approx \sum_{i=1}^{15} w_i \frac{t_1 - t_0}{2} g\left(\frac{x_i + 1}{2}(t_1 - t_0) + t_0\right) \tag{10}$$

(10) can be used to calculate the arc length of the lane curve, which is not only used for equidistant sampling but also in intersection steering scenarios. The arc length can also be used to calculate curvature, which is convenient for planning.

5. LOCALIZATION BASED ON AN HD MAP

There are a variety of complex road environments in the cities, such as tunnels, overpasses, and urban canyons. These environments make GNSS-based localization less reliable. Some odometry fusing methods have emerged to solve the problem of GNSS failure. However, due to odometry drift, these methods cannot meet the localization requirements in scenarios where there is a long-term lack of effective global position information [34]. Although point cloud map relocalization based on the iterative closest point (ICP) [35], normal distribution transform (NDT) [36] and other methods is very effective, a very large point cloud map becomes a major challenge that affects practical use. An HD map contains various semantic features, while lane lines and traffic signs have good recognition both day and night. To explore the global localization method combining an HD map and IMU, two problems need to be solved. First, the elements in the HD map are associated with the elements detected using other sensors. Second, the pose is estimated based on the feature association results.

5.1. Reprojection

Reprojection refers to projecting the coordinates of a corresponding point in 3D space back to the pixel plane according to the currently estimated pose. The error between the reprojected and actual pixel coordinates is called the reprojection error and is often used as an indicator to evaluate the pose. Based on the position of the lane in the map, the known a priori knowledge of the HD map is projected onto the camera image by combining the intrinsic and extrinsic parameters of the camera. The evaluation of a pose metric is obtained by differencing the a priori map element positions and the coordinates of the matching perceptual results. Ideally, the distance between the two should be zero. The optimal camera pose can be obtained by optimizing the camera pose using a nonlinear optimization method to minimize this evaluation metric so that the optimal vehicle pose can be calculated.

First, referring to the transcendental vehicle pose $\boldsymbol{T}_{\mathrm{bw}}$, combined with (3), the representation of a feature point

$\boldsymbol{P}_{\mathrm{w}}$ in the world coordinate system at the coordinates $\boldsymbol{P}_{\mathrm{uv}}$ in the pixel plane system can be obtained.

$$\boldsymbol{p}_{uv} = h(\boldsymbol{T}_{\mathrm{bw}}, \boldsymbol{p}_{\mathrm{w}}) = \frac{1}{Z_c}\boldsymbol{K}\boldsymbol{T}_{\mathrm{cb}}\boldsymbol{T}_{\mathrm{bw}}\boldsymbol{p}_{\mathrm{w}} \tag{11}$$

where $\boldsymbol{T}_{\mathrm{cb}}$ is the transformation matrix from the vehicle coordinate system to the camera coordinate system, $\boldsymbol{T}_{\mathrm{bw}}$ is the transformation matrix from the world coordinate system to the vehicle coordinate system, and Z_c is the z axis coordinate of the feature point in the camera coordinate system, K is the camera internal parameter matrix. According to (11), the elements in the HD map are projected into the pixel plane.

5.2. Feature association

To use an HD map for localization, the location of objects detected by the sensors on the HD map needs to be known. This step is called feature association. Feature association locates HD map elements that match the features detected in the camera images. The correct selection of map features can significantly improve the localization results. In this study, we choose lane line elements as map features. This is because lane line features are easy to detect, have a long duration, and have good reflection properties, and have a high detection success rate in environments such as nighttime. The map elements are reprojected to the pixel plane (map features), and the distance between the detected elements (perceptual features) is calculated and used to evaluate the localization results.

Define the perceptual feature x as consisting of kind x^l and shape x^b, i.e. $x = \{x^l, x^b\}$. For lane line perception feature x, the slope difference of lanes on the same road section is very small. There is a possibility that distant lanes may be included in the HD map reprojection process by mistake. To better distinguish lane lines on the same road section, the shape is defined to consist of a sequence of lane line points x^s and their slopes x^d: $x^b = \{x^s, x^d\}$.

Based on the consistency of the local structure, the map feature reprojection error is calculated. Then, coarse matching of features and HD map perceptual features is performed. If the reprojection error is too large, the gap between the map and perceptual features is considered too large and will not be matched and optimized. The algorithm continues only when the error is less than a certain threshold. Define the map feature as y and given camera perceptual feature x, consider the confidence x^c that a feature belongs to a certain class with probability $P(x^l|y^l)$ given by the target detection module. Assuming that the shape detection noise obeys a normal distribution, this is combined with computing the feature's likelihood probability $P(x|y)$.

$$P(x|y) = P(x^l|y^l)P(x^c|y^l, x^l)P(x^b|y^b) \tag{12}$$

For the lane lines, define the likelihood probability $P(x^b|y^b)$ of the shape.

$$P(x^b|y^b) = \omega e^{-\frac{1}{2}\left(\frac{x_i^d - y_i^d}{\sigma_d}\right)^2} + (1-\omega)e^{-\frac{1}{2}\left(\frac{\bar{x}^p - \bar{y}^p}{\sigma_p}\right)^2} \tag{13}$$

where y^d and x^d are the slopes of the lane lines in the map feature and the perceptual feature, respectively, and $\bar{x}^p$ and $\bar{y}^p$ are the average coordinates of the sampling points of the lane lines on the x-axis in the map feature and the perceptual feature, respectively. σ_d is the variance of the lane slope. If the likelihood probability $P(x|y)$ is greater than a certain threshold Th, this map feature and the perceptual feature are considered as a pair of coarse matches $z_{ij} = \{x_i, y_j\}$ for the same feature.

Considering the map structure consistency, the perceptual feature structure should be similar to the map feature structure. After coarse matching, the distance between two of each map feature and the distance between two of the matching perceptual features is calculated, as shown in Figure 4. These two sets of distances are

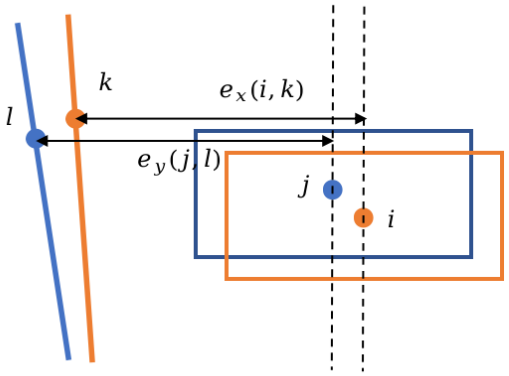

Figure 4. Edge similarity definition

called the structural features of the map features and the structural features of the perceptual features. The difference in the structural features is used as a measure to assess the similarity between a given frame's perceptual feature structure and the map feature structure.

Define the matching matrix $\boldsymbol{D} \in \mathbb{R}^{N_n \times N_m}$, where the element $d_{ij} = 1$ indicates that the perceptual feature x_i matches the map feature y_j; otherwise, $d_{ij} = 0$. Define that in two feature pairs d_{ij} and d_{kl}, the edge $e_x(i,k)$ denotes the horizontal distance between perceptual features x_i and x_k, and similarly, the edge $e_y(j,l)$ denotes the horizontal distance between map features y_j and y_l. Then, the similarity between the perceptual feature structure and map feature structure s_t in a certain frame is shown in (14).

$$s = \frac{1}{N_e} \sum_{i=1}^{N_n} \sum_{j=1}^{N_m} \sum_{k=1}^{N_n} \sum_{l=1}^{N_m} d_{ij} d_{kl} \exp\left(\left(\frac{e_y(j,l) - e_x(i,k)}{2\sigma_e} \right)^2 \right) \tag{14}$$

where N_n and N_m are the total numbers of perceptual features and map features after reprojection, respectively. $d_{ij}d_{kl}$ denotes the requirement that this edge exists for both map features and perceptual features. N_e is the number of all possible edges that satisfy the above requirement.

Considering the number of matches, structural consistency, and reprojection error, the feature matching problem can be expressed as a multi-order map matching problem.

$$\hat{\boldsymbol{D}} = \arg\max_{\boldsymbol{D}} \ \omega_1 N_d + \omega_2 s + \omega_3 \frac{1}{N_d} \sum_{i=1}^{N_n} \sum_{j=1}^{N_m} d_{ij} P(x_i | y_j) \tag{15}$$

where N_d is the number of feature matching pairs. $P(x_i|y_j)$ and s can be calculated by (12) and (15). ω_1, ω_2, ω_3 are the weight parameters.

5.3. Factor graph optimization

Define known sensor measurements $Z = \{z_i\}_{i=1}^{N_z}$, map feature measurements $Y = \{y_j\}_{j=1}^{N_m}$, where $l_j \in \mathbb{R}^3$, and pose estimates $X = \{x_t\}_{t=1}^{N_x}$, where $x_t \in SE(2)$. The HD map-based localization can be expressed as a maximum a posteriori probability (MAP) estimation as follows:

$$\hat{X} = \arg\max_{X} P(X|Z,Y) \tag{16}$$

This MAP estimation can be decomposed into two subproblems, feature association and pose estimation, to

create a feature association $D = \{d_t\}_{t=1}^{N_d}$ between the perceptual measurements and map feature measurements. It is obtained as follows:

$$\hat{X}, \hat{D} = \arg\max_{X,D} P(X, D|Z, Y) = \arg\max_{X,D} P(X|D, Z, Y)P(D|X, Z, Y) \tag{17}$$

We use factor graphs to optimally fuse odometry z^o and map feature measurements z^l from feature matching. It is more difficult to solve the posterior distribution directly, and with the matching relationship $\hat{D}$ already estimated, using Bayes' theorem, (17) can be written as

$$\hat{X} = \arg\max_{X} P(X|Z, Y, \hat{D}) = \arg\max_{X} P(X)P(Z|X, Y, \hat{D}) \tag{18}$$

The above equation splits the MAP estimation into the product of the maximum likelihood estimate (MLE) and the prior. Therefore, (17) can be equated to an MLE problem. Therefore, the pose X optimization problem can be constructed based on the odometry z^o and the feature matching pair (called landmarks) z^l obtained in the previous section. The error term consists of the odometry error e^o and the observation error e^y. The observation error e^y can be composed of the coordinate error e^l of the landmark and the map error e_j^m. Therefore, we divide the error term into three parts: odometry error e^o, landmark error e^l and map error e_j^m.

Assume that the noise satisfies a normal distribution. The odometry error optimization term can be defined as:

$$\sum_k e^o(x_{k-1}, x_k, z_k^o)^{\mathrm{T}} \Omega_k^o e^o(x_{k-1}, x_k, z_k^o) \tag{19}$$

where Ω_k^o is the information matrix, and the odometry error $e^o(x_{k-1}^p, x_k^p, z_k^o)$ can be expressed as the difference between the current pose $x_k^{p\mathrm{T}}$ after performing the transformation z_k^o on the pose x_{k-1}^p for the previous frame:

$$e^o(x_{k-1}^p, x_k^p, z_k^o) = x_k^{p\mathrm{T}} x_{k-1}^p z_k^o \tag{20}$$

The landmark error optimization term can be defined as:

$$\sum_k e^l(x_k^p, x^l, z_k^l)^T \Omega_k^l e^l(x_k^p, x^l, z_k^l) \tag{21}$$

where the landmark error can be represented by the difference between the x-axis coordinates of the perceptual features and map features:

$$e^l(x_k^p, x^l, z_k^l)^{\mathrm{T}} = \left[\frac{1}{Z_k^c} \boldsymbol{K} \boldsymbol{T}_{\mathrm{cb}} x_k^{p\mathrm{T}} x^l - z_k^l \right]_0 \tag{22}$$

The map error optimization term can be described as[37]:

$$\sum_k e_k^m(x^l)^{\mathrm{T}} \Omega_k^m e_k^m(x^l) = \frac{\gamma(c)}{r^2} \sum_k (x^l - m_k)^{\mathrm{T}} (x^l - m_k) \tag{23}$$

where $\gamma(c)$ is the inverse-chi-squared distribution function, r is the radius, and m_k is the location of the kth frame map feature.

When the error of a particular edge is significant, the growth rate of the Mahalanobis distance in the above equation is substantial. Therefore, the algorithm will try to preferentially adjust the estimates associated with this edge and ignore the effect of other advantages. This study uses the Huber kernel function $H(x)$ to adjust the error term and reduce the impact of erroneous data.

Combining (19), (21), and (23), the pose optimization function is obtained as follows:

$$\begin{aligned}\hat{X} = \arg\min_{X} \sum_{k} H\left(e^{o}(x_{k-1}^{p}, x_{k}^{p}, z_{k}^{o})^{\mathrm{T}} \Omega_{k}^{o} e^{o}(x_{k}^{p}, x_{k}^{p}, z_{k}^{o})\right) \\ + \sum_{k} H\left(e^{l}(x_{k}^{p}, x^{l}, z_{k}^{l})^{\mathrm{T}} \Omega_{k}^{l} e^{l}(x_{k}^{p}, x^{l}, z_{k}^{l})\right) \\ + \frac{\gamma(c)}{r^{2}} \sum_{k} (x^{l} - m_{k})^{\mathrm{T}} (x^{l} - m_{k})\end{aligned} \tag{24}$$

6. EXPERIMENTS AND RESULTS

We validated the proposed localization algorithm through a series of experiments. First, the KITTI dataset is gradually simplified to fit a single parametric curve based on various lane characteristics. The curve equation of each lane line is calculated based on the three-time Hermite spline curve fitting algorithm proposed in this paper. Then, after intersection complementation and manual adjustment of elements, an HD map corresponding to the KITTI dataset is generated. Finally, based on the original odometry, the priori HD map information and the fused HD map localization algorithm proposed are used to further constrain the vehicle's lateral position.

6.1. Curve fitting

To fit the lane lines, we must extract the lane points. The first step uses the ground plane fitting (GPF) algorithm [30] to calculate the ground equation. The coordinates of the lane lines on the image in the camera coordinate system $\boldsymbol{P}_{\mathrm{c}}$ are calculated according to (5). Using the localization data of the GNSS/INS system as vehicle position true value $\boldsymbol{P}_{\mathrm{b}}$, the lane line recognition results of each frame are stitched and the same road section with different lane lines are stored as different categories. The StatisticalOutlierRemoval (SOR) filter [38] is used to filter some misdetected outliers. This step also excludes some poorly detected road sections together, which are reflected as different colors in different lane line maps, as shown in Figure 5(a).

The second step uses density-based spatial clustering of applications with noise (DBSCAN) [39] clustering to divide the closely spaced points (distance less than a certain threshold) into the same cluster. This search threshold needs to be slightly greater than the lane spacing and less than the distance between adjacent lanes at an intersection. This enables the clustering algorithm to search for adjacent lanes and ensure that the intersection area can be used for segmentation. Because of the large number of point clouds, the KD-Tree search algorithm is used rather than a traditional traversal search. Through DBSCAN clustering, the lane lines are divided into 19 areas, as shown in Figure 5(b).

In the third step, the lanes are divided via DBSCAN clustering using the information of different lanes in the same road recorded in the first step. Then the lanes are divided according to the category attribute for each segment, as shown in Figure 5(c). A unique ID is assigned to each lane here for subsequent lane completion.

The curve fitting process is shown in Figure 6, where the upper left, middle and right are X-Y, X-Z, and Y-Z views, respectively, which show that the fitting effect is relatively good. The spatial curve can describe the original lane line point set better.

The middle subplot of Figure 6 shows the fitting effect of parameter t, indicating the variation of the error of all parameters $\boldsymbol{t}_{\mathrm{i}}$ with the number of iterations. After four iterations, the error of most parameters $\boldsymbol{t}_{\mathrm{i}}$ decreases to below 1.0. The lower subplot shows the variation of the total error during the iterative calculation, and the error is stable after two iterations. The 3D view of this lane line fitting effect is shown in Figure 7.

This study determines the intersection connection based on the vehicle path to solve the problem that there

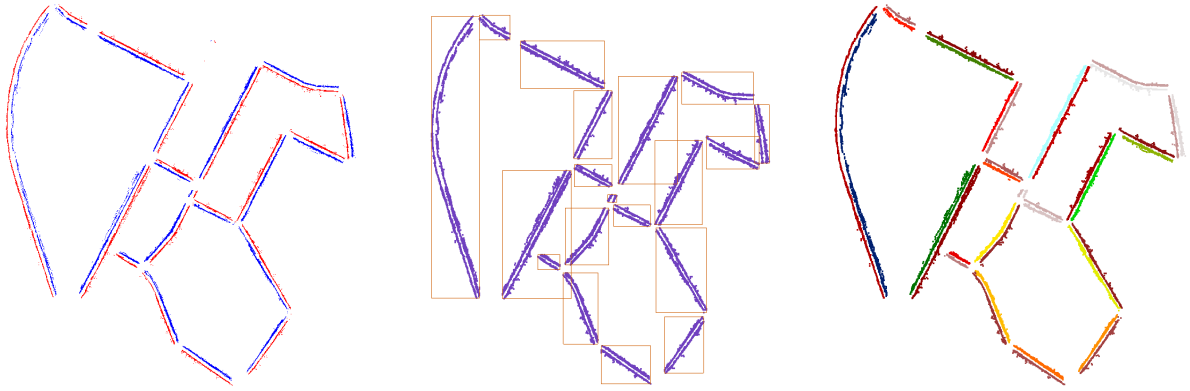

(a) Original lane data (b) Cluster division of lane (c) Cluster division with class

Figure 5. Extract lane points.

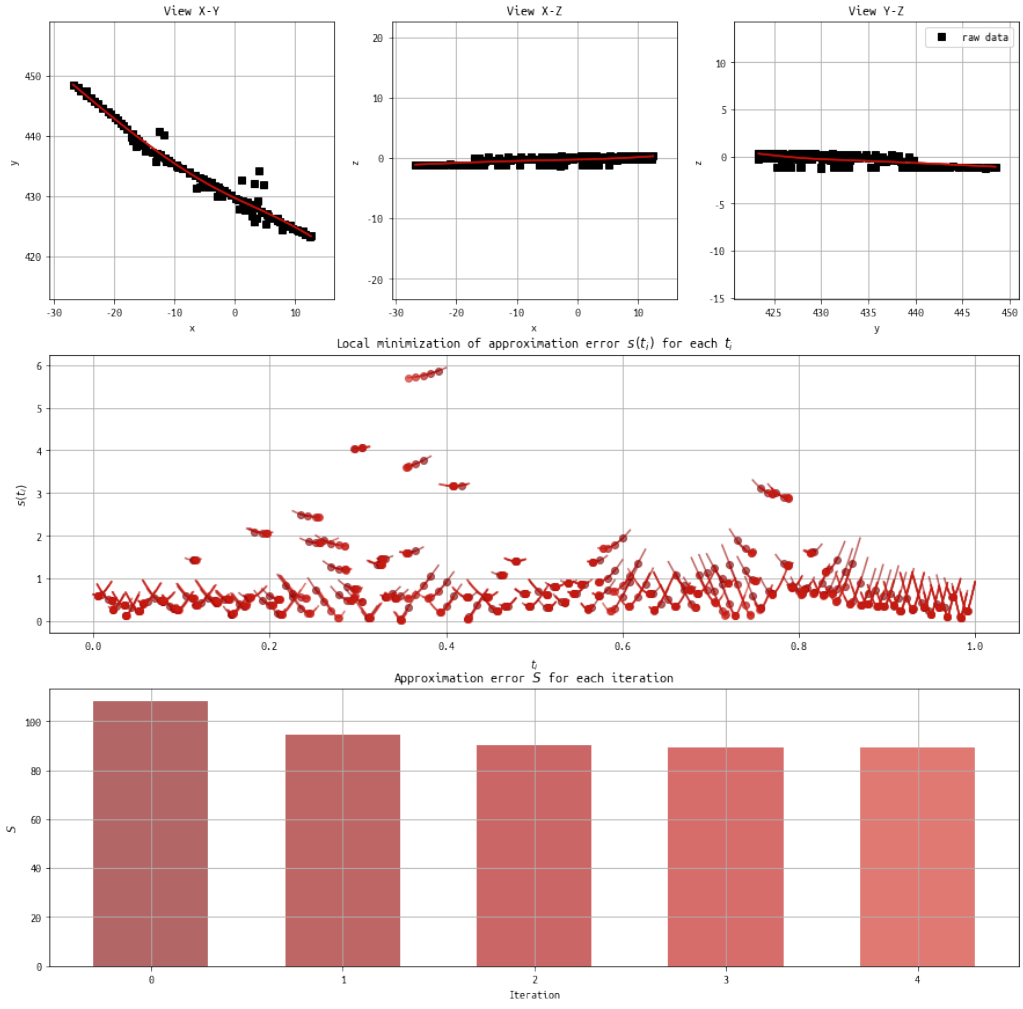

Figure 6. Curve fitting process.

may be no left turn or right turn on the road. The intersection topology is selected by combining the IDs assigned to each lane. The algorithm completes the virtual lane lines of the intersection.

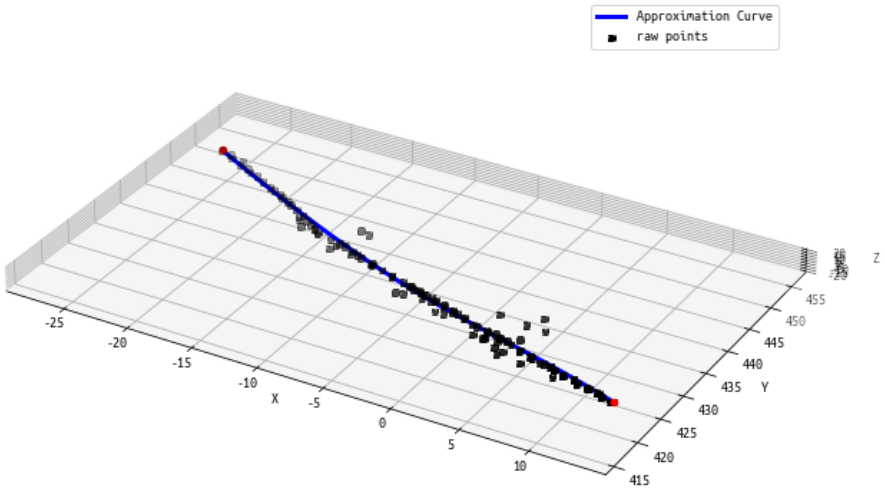

Figure 7. Single lane fitting result.

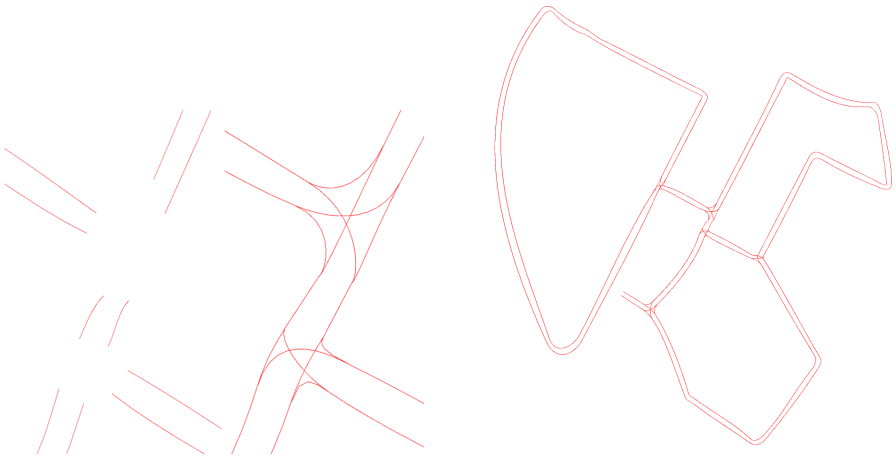

(a) Crossing fitting before and after comparison (b) Global lane fitting result

Figure 8. Lane Fitting Process

The results before and after intersection completion are shown in Figure 8(a). The final lanes for the entire area are shown in Figure 8(b), and the overall lane fit is relatively good. To create an HD map, further manual adjustment of the lane curve is also required, and complements other elements on the map, such as sidewalks and various traffic signs.

6.2. HD map production

The vehicle's starting point is defined as the map origin, and the GPS coordinates of the origin (48.982 545 °W, 8.390 366 °E) are recorded. To obtain higher projection accuracy, the European ETRS89 coordinates are used in this study. The coordinate system parameters are shown in Table 1.

We import the long-axis flattening of the Earth ellipsoid defined by the ETRS coordinate system in Table 1 into the Geographiclib geographic coordinate library for calculation. The coordinates of the initial point in the MGRS geographic coordinate system are 32UMV-55394.36-25694.44, of which the area number is 32UMV, the distance to the east is 55394.36 m, the distance to the north is 25 694.44 m, and the grid north angle is −0.5°.

Table 1. ETRS89 coordinate System

Name	Value
EPSG number	EPSG:25832
Prime meridian	Greenwich
Earth's ellipsoid	GRS 1980 (long axis: 6,378,137 m, flat rate: 298.257,222)

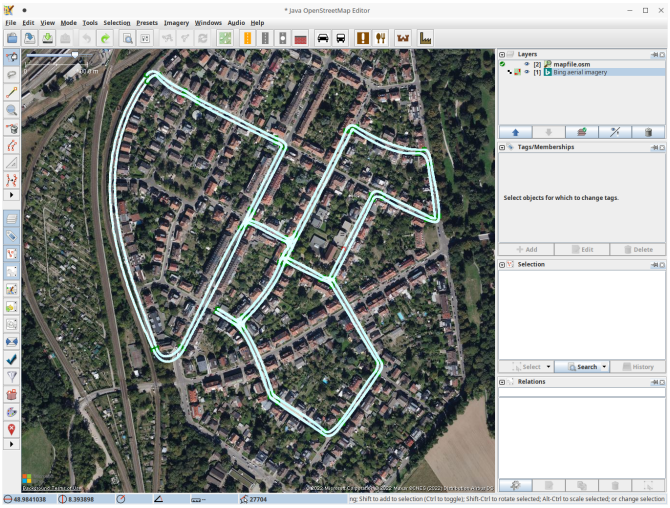

Figure 9. The lanelet2 map.

The MGRS coordinates of the lane lines and initial points shown in Figure 8(b) are stored in the Lanelet2 file. After opening the Lanelet2 file with the JOSM professional map software, the Mapbox satellite map is loaded as the base map. As shown in Figure 9, the converted coordinates can be recognized and displayed correctly by the professional mapping software. The road shapes overlap with the roads in the satellite map.

Figure 8(b) shows that some intersections are poorly fitted. The elements, such as stop lines and crosswalks, are not identified. Therefore, some elements that were missed by mistake were manually adjusted, the lane shape was fine-tuned, and pedestrian crossing markings and some traffic signs were added. Figure 10 shows the effect of manual labeling of some intersections. After adjusting the lane lines, a new curve equation needs to be refitted for this lane using the method in Part IV. Finally, the lane curve is optimized using a numerical integration method to approximate the arc-length isometric sampling.

6.3. Localization experiment

Following the previous preparations, the next step is to conduct a localization experiment. The points of the HD map are projected in the image coordinate system using formula (11). Considering the actual lanes in the camera image orientation, only the lanes located in the lower half of the image are kept, as shown in Figure 11. Since the virtual lane (blue) in the figure should not be involved in matching and optimizing the position attitude, only the actual lane (red) is reserved for lane matching and position optimization. The horizontal red lanes on both sides result from the projection of the nearby road, not the current road. The algorithm filters the possible lanes by radius and then projects them into the image. The final lanes involved in matching are shown in Figure 12.

Because the inertial guidance odometry in the KITTI dataset is relatively accurate, it does not reflect the effect of the localization algorithm well. In this paper, we use the LOAM [22] algorithm as a laser odometry and match the HD map with the actual detection results using the method proposed in Part V. The obtained matching results are added to the Georgia Tech Smoothing and Mapping (GTSAM) [40] optimization as roadmap con-

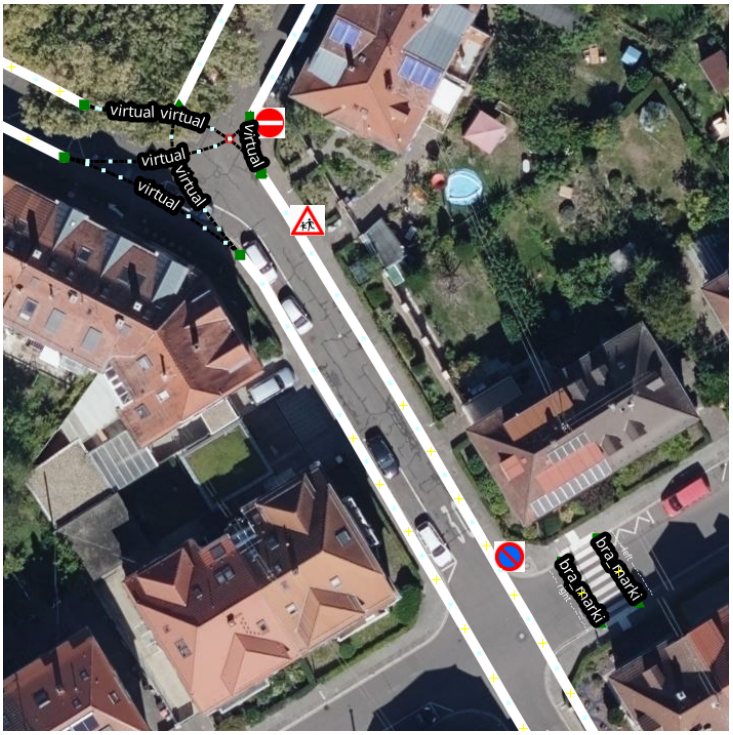

Figure 10. Manual marking.

Figure 11. The reprojection of HD map.

Figure 12. Available lanes for matching and optimizationp.

straints. To test the effect of fused localization, the fused HD map localization algorithm designed in this study is compared with the comparison of the actual value, as shown in Figure 13.

The metric commonly used in academia to evaluate trajectories is the root-mean-square deviation (RMSE):

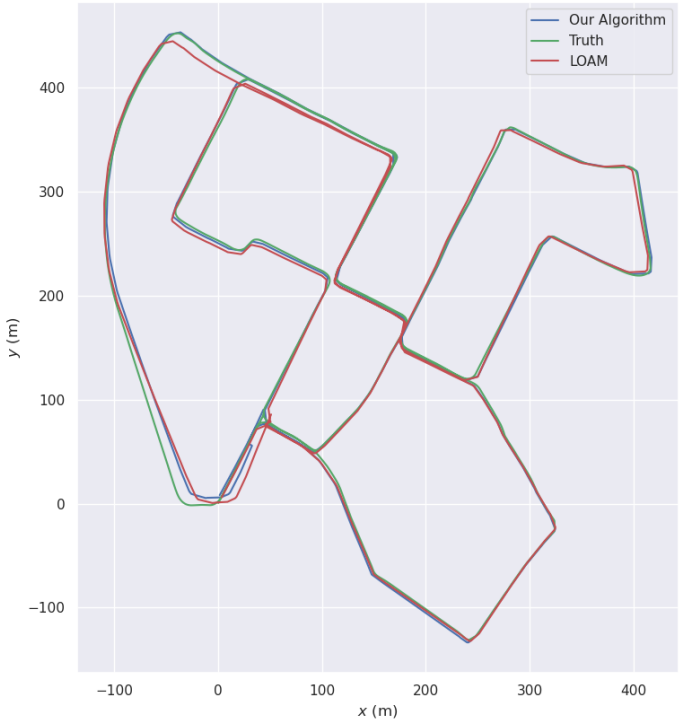

Figure 13. Comparison between our algorithm, LOAM and the ground truth.

Table 2. Localization error

Algorithm	RMSE	Min APE error	Max APE error
Algorithm of this paper	4.3361m	0.6679m	15.1492m
LOAM	12.5518m	1.1545m	21.8804m

$$\mathrm{RMSE} = \sqrt{\frac{1}{N}\sum_{i=1}^{N}\mathrm{APE}^2} \tag{25}$$

The absolute pose error (APE) considers only translational errors:

$$\mathrm{APE} = \left\|\mathrm{trans}(\boldsymbol{T}_{gt,i}^{-1}\boldsymbol{T}_{est,i})\right\| \tag{26}$$

In this study, the EVO [41] toolkit is used to evaluate the trajectory error of the proposed localization algorithm, and the results are shown in Table 2.

Figure 13 shows the comparison of the effect of the proposed algorithm and the LOAM algorithm. The proposed localization algorithm has a more significant improvement compared to the pure LOAM distance meter. As seen, the error in the localization effect of incorporating the HD map remains small most of the time. A horizontal offset can be seen in the upper left part of the road where the HD map does not exist. Because the leftmost road is long and has a particular curvature, the localization of the fused HD map needs to be improved for the forward direction. The LiDAR odometer has a large offset on the lower left side of the road,

(a) Experimental scenes

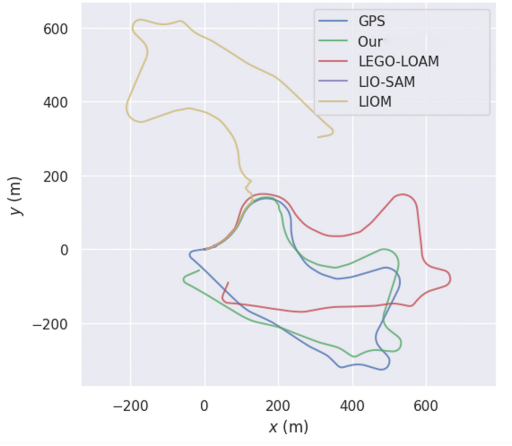

(b) Localization results

Figure 14. Robustness test.

so the algorithm developed in this study also has a large offset. This problem can be solved by subsequently considering adding more road elements.

6.4. Robustness test

Now, we compare the localization performance of the method in this paper with other methods. Since the road in the experimental scenes is lined with trees, the features extracted by LiDAR from the dense foliage are very noisy. In the experimental scenes, the GPS localization is correct because the GPS signal completely covers the experimental data set. We treat the GPS measurements here as ground truth. Figure 14(b) shows the localization results of the method in this paper with other methods in this case. LIOM lacks a pre-processing method to filter out reliable features, so its results are far from the correct ones. The unsatisfactory LIO-SAM results are due to unreliable features that severely affect the matching between keyframes. The method in this paper can obtain more accurate results than other methods.

7. CONCLUSION

In this paper, an iterative approximation-based method is proposed to generate the 3D curves of lane lines. For the problem of uneven sampling points in HD maps, a method based on numerical integration is proposed to achieve uniform sampling over the arc length. Based on the feature association results of the HD map and the perceptual image, lateral constraints are applied to the odometer localization results to obtain accurate and low-cost localization results. Experimental results show that the proposed method can generate HD maps and achieve high-precision localization. Future work will try to consider the lateral serial numbers of lane lines for clustering. Larger thresholds are easier to cluster on lane points with the same serial number. The radius threshold of lane points with different serial numbers is reduced so that the clustering can be clustered along the direction of lane lines, which can solve the problem of intermittent lane lines. To improve the practicality of this method, we will continue to explore the detection of more road elements, the generation of topological relationships for complex road sections (e.g., traffic circles), and the automatic association methods of traffic signs and lanes in the future. The main sensors used in this system are LiDAR and camera, which are sensitive to rain and snow occlusion. Therefore, the present system is not robust in rain and snow environment. In the subsequent work, thanks to the graphical optimization framework, we can easily add GPS measurement constraints to the position map. This can overcome the effect of rain and snow environment on the system to some extent. Cloudy weather is still one of the important challenges for GPS localization systems. In future

work, we will add kinematic model constraints to improve GPS localization results.

DECLARATIONS

Authors' contributions

Writing-Original Draft and conceptualization: Huang Z
Technical Support: Chen S
Validation and supervision: Xi X, Li Y
Investigation: Li Y, Wu S

Availability of data and materials

Not applicable.

Financial support and sponsorship

This work was supported by the Open fund of State Key Laboratory of Acoustics under Grant SKLA202215.

Conflicts of interest

All authors declared that there are no conflicts of interest

Ethical approval and consent to participate

Not applicable

Consent for publication

Not applicable

REFERENCES

1. Jeong J, Cho Y, Shin YS, Roh H, Kim A. Complex urban dataset with multi-level sensors from highly diverse urban environments. *Int J Robot Res* 2019;38:642-57. DOI
2. Azimi SM, Fischer P, Körner M, Reinartz P. Aerial LaneNet: lane-marking semantic segmentation in aerial imagery using wavelet-enhanced cost-sensitive symmetric fully convolutional neural networks. *IEEE Trans Geosci Remote Sensing* 2019;57:2920-38. DOI
3. Fischer P, Azimi SM, Roschlaub R, Krauß T. Towards HD maps from aerial imagery: robust lane marking segmentation using country-scale imagery. *IJGI* 2018;7:458. DOI
4. Cheng W, Yang S, Zhou M, et al. Road Mapping and Localization Using Sparse Semantic Visual Features. *IEEE Robot Autom Lett* 2021;6:8118-25. DOI
5. Qin T, Zheng Y, Chen T, Chen Y, Su Q. RoadMap: A light-weight semantic map for visual localization towards autonomous driving. arXiv:210602527 [cs] 2021 Jun. Available from: http://arxiv.org/abs/2106.02527. [Last accessed on 29 Jan 2023]
6. Hosseinyalamdary S, Peter M. LANE LEVEL LOCALIZATION; USING IMAGES AND HD MAPS TO MITIGATE THE LATERAL ERROR. *Int Arch Photogramm Remote Sens Spatial Inf Sci* 2017;XLII-1/W1:129-34. DOI
7. Matthaei R, Bagschik G, Maurer M. Map-relative localization in lane-level maps for ADAS and autonomous driving. In: 2014 IEEE Intelligent Vehicles Symposium Proceedings. MI, USA: IEEE; 2014. pp. 49–55. Available from: http://ieeexplore.ieee.org/document/6856428/. [Last accessed on 29 Jan 2023]
8. Nedevschi S, Popescu V, Danescu R, Marita T, Oniga F. Accurate Ego-Vehicle Global Localization at Intersections Through Alignment of Visual Data With Digital Map. *IEEE Trans Intell Transport Syst* 2013;14:673-87. DOI
9. Qu X, Soheilian B, Paparoditis N. Vehicle localization using mono-camera and geo-referenced traffic signs. In: 2015 IEEE Intelligent Vehicles Symposium (IV); 2015. pp. 605–10. DOI
10. Tao Z, Bonnifait P, Frémont V, Ibañez-Guzman J. Mapping and localization using GPS, lane markings and proprioceptive sensors. In: 2013 IEEE/RSJ International Conference on Intelligent Robots and Systems; 2013. pp. 406–12. DOI
11. Welzel A, Reisdorf P, Wanielik G. Improving urban vehicle localization with traffic sign recognition. In: 2015 IEEE 18th International Conference on Intelligent Transportation Systems; 2015. p. 5. DOI
12. Xiao Z, Yang D, Wen T, Jiang K, Yan R. Monocular Localization with Vector HD Map (MLVHM): A Low-Cost Method for Commercial IVs. *Sensors (Basel)* 2020;20:1870. DOI

13. Jo K, Lee M, Kim C, Sunwoo M. Construction process of a three-dimensional roadway geometry map for autonomous driving. *Proceedings of the Institution of Mechanical Engineers, Part D: Journal of Automobile Engineering* 2017;231:1414-34. DOI
14. Chen A, Ramanandan A, Farrell JA. High-precision lane-Level road map building for vehicle navigation. In: IEEE/ION Position, Location and Navigation Symposium; 2010. pp. 1035–42. DOI
15. Jo K, Sunwoo M. Generation of a precise roadway map for autonomous cars. *IEEE Trans Intell Transport Syst* 2014;15:925-37. DOI
16. Zhang T, Arrigoni S, Garozzo M, Yang Dg, Cheli F. A lane-level road network model with global continuity. *Transportation Research Part C: Emerging Technologies* 2016;71:32-50. DOI
17. Gwon GP, Hur WS, Kim SW, Seo SW. Generation of a precise and efficient lane-level road map for intelligent vehicle systems. *IEEE Trans Veh Technol* 2017;66:4517-33. DOI
18. Godoy J, Artuñedo A, Villagra J. Self-Generated OSM-Based Driving Corridors. *IEEE Access* 2019;7:20113-25. DOI
19. Jiang K, Yang D, Liu C, Zhang T, Xiao Z. A flexible multi-layer map model designed for lane-level route planning in autonomous vehicles. *Engineering* 2019;5:305-18. DOI
20. Poggenhans F, Pauls JH, Janosovits J, et al. Lanelet2: a high-definition map framework for the future of automated driving. In: 2018 21st International Conference on Intelligent Transportation Systems (ITSC). Maui, HI: IEEE; 2018. pp. 1672–79. Available from: https://ieeexplore.ieee.org/document/8569929/. [Last accessed on 29 Jan 2023]
21. Marais J, Ambellouis S, Flancquart A, et al. Accurate localisation based on GNSS and propagation knowledge for safe applications in guided transport. *Procedia - Social and Behavioral Sciences* 2012;48:796-805. DOI
22. Zhang J, Singh S. LOAM: Lidar odometry and mapping in real-time. In: Robotics: Science and Systems. vol. 2. Berkeley, CA; 2014. pp. 1–9.
23. Shan T, Englot B. Lego-loam: Lightweight and ground-optimized lidar odometry and mapping on variable terrain. In: 2018 IEEE/RSJ International Conference on Intelligent Robots and Systems (IROS). IEEE; 2018. pp. 4758–65. DOI
24. Qin C, Ye H, Pranata CE, et al. LINS: a lidar-inertial state estimator for robust and efficient navigation. In: 2020 IEEE International Conference on Robotics and Automation (ICRA). IEEE; 2020. pp. 8899–906. DOI
25. Shan T, Englot B, Meyers D, et al. Lio-sam: Tightly-coupled lidar inertial odometry via smoothing and mapping. In: 2020 IEEE/RSJ International Conference on Intelligent Robots and Systems (IROS). IEEE; 2020. pp. 5135–42. DOI
26. Campos C, Elvira R, Rodríguez JJG, M Montiel JM, D Tardós J. ORB-SLAM3: an accurate open-source library for visual, visual–inertial, and multimap SLAM. *IEEE Trans Robot* 2021;37:1874-90 DOI
27. Qin T, Li P, Shen S. Vins-mono: A robust and versatile monocular visual-inertial state estimator. *IEEE Trans Robot* 2018;34:1004-20. DOI
28. Qin T, Shen S. Online temporal calibration for monocular visual-inertial systems. In: 2018 IEEE/RSJ International Conference on Intelligent Robots and Systems (IROS). IEEE; 2018. pp. 3662–69. DOI
29. Geiger A, Lenz P, Stiller C, Urtasun R. Vision meets robotics: the KITTI dataset. *Int J Robot Res* 2013;32:1231–37. DOI
30. Zermas D, Izzat I, Papanikolopoulos N. Fast segmentation of 3D point clouds: a paradigm on LiDAR data for autonomous vehicle applications. In: 2017 IEEE International Conference on Robotics and Automation (ICRA). Singapore, Singapore: IEEE; 2017. pp. 5067–73. Available from: http://ieeexplore.ieee.org/document/7989591/. [Last accessed on 29 Jan 2023]
31. Byrd RH, Lu P, Nocedal J, Zhu C. A limited memory algorithm for bound constrained optimization. *SIAM J Sci Comput* 1995;16:1190-208. DOI
32. Fritsch FN, Carlson RE. Monotone piecewise cubic interpolation. *SIAM J Numer Anal* 1980;17:238-46. DOI
33. Kronrod AS. Nodes and weights of quadrature formulas. New York: Consultants Bureau 1965. DOI
34. Wang H, Xue C, Zhou Y, Wen F, Zhang H. Visual semantic localization based on HD map for autonomous vehicles in urban scenarios. In: 2021 IEEE International Conference on Robotics and Automation (ICRA). Xi'an, China: IEEE; 2021. pp. 11255–61. Available from: https://ieeexplore.ieee.org/document/9561459/. [Last accessed on 29 Jan 2023]
35. Besl PJ, McKay ND. Method for registration of 3-D shapes. In: Sensor fusion IV: control paradigms and data structures. vol. 1611. Spie; 1992. pp. 586–606. DOI
36. Biber P, Straßer W. The normal distributions transform: a new approach to laser scan matching. In: Proceedings 2003 IEEE/RSJ International Conference on Intelligent Robots and Systems (IROS 2003)(Cat. No. 03CH37453). vol. 3. IEEE; 2003. pp. 2743–48. DOI
37. Wilbers D, Merfels C, Stachniss C. Localization with sliding window factor graphs on third-Party maps for automated driving. In: 2019 International Conference on Robotics and Automation (ICRA). Montreal, QC, Canada: IEEE; 2019. pp. 5951–57. Available from: https://ieeexplore.ieee.org/document/8793971/. [Last accessed on 29 Jan 2023]
38. Rusu RB, Marton ZC, Blodow N, Dolha M, Beetz M. Towards 3D Point cloud based object maps for household environments. *Robot Auton Syst* 2008;56:927-41. DOI
39. Ester M, Kriegel HP, Sander J, Xu X. A density-Based algorithm for discovering clusters in large spatial databases with noise. In: Proceedings of the Second International Conference on Knowledge Discovery and Data Mining. KDD'96. AAAI Press; 1996. pp. 226–31. DOI
40. Dellaert F. Factor graphs and GTSAM: a hands-on introduction. Georgia Institute of Technology; 2012. DOI
41. Grupp M. Evo: Python package for the evaluation of odometry and SLAM.; 2017. Available from: https://github.com/MichaelGrupp/evo. [Last accessed on 29 Jan 2023]